The Blazar Sequence and the Cosmic Gamma-ray Background Radiation in the Fermi Era

Yoshiyuki Inoue and Tomonori Totani,
arXiv:0810.3580

Masaki Mori

ICRR CANGAROO group internal seminar, November 28, 2008

Strong, Moskalenko & Reimer, ApJ 613, 956

Extragalactic diffuse gamma-ray background

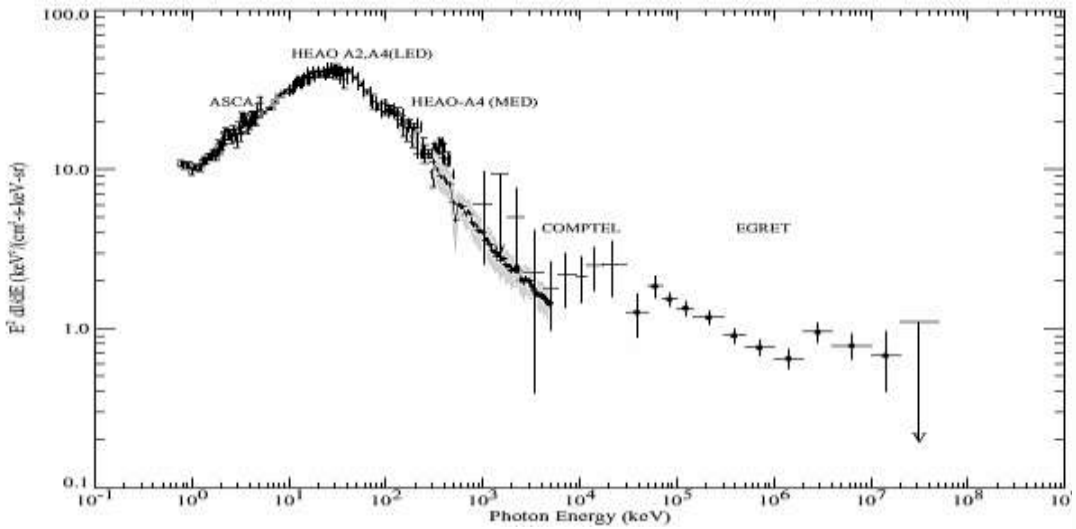

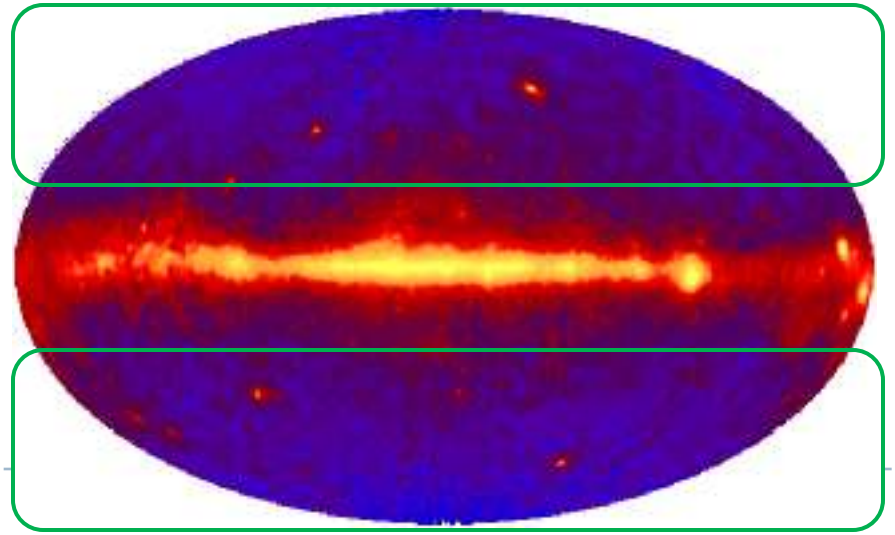

EGRET allsky map

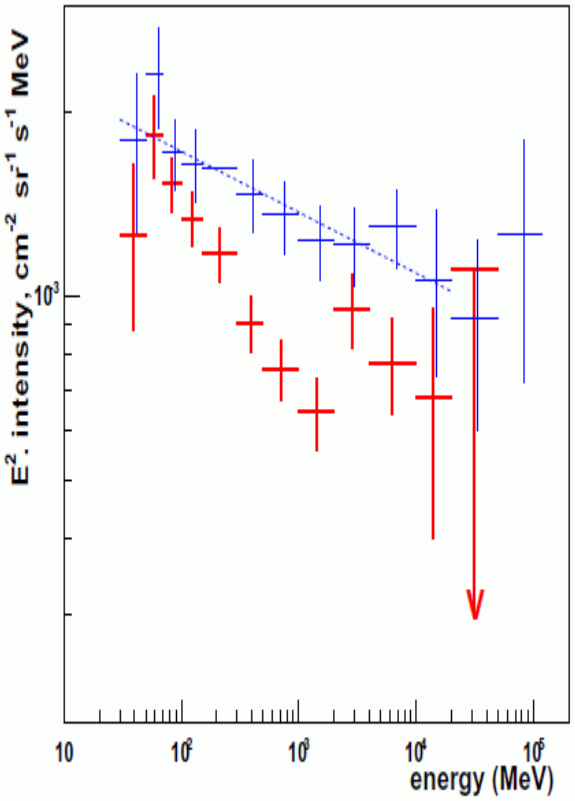

FIG. 2.— Comparison of our EGRB spectrum (solid, red) as given in Table 3 with that from Sreekumar et al. (1998) (dots, magenta). The dashed (blue) line is the Sreekumar et al. fit: $2.743 \times 10^{-3} E^{-2.1}$ cm^{-2} s^{-1} sr^{-1} MeV^{-1}.

Origin of EGBR

- Clusters of galaxies?
- Dark matter annihilation?
- Blazars?
  - Most of EGRET-detected extragalactic sources are blazars?!
    - Stecker & Salamon (1996)
    - Chiang and Mukherjee (1998)
    - Mücke & Pohl (2000)
    - Narumoto & Totani (2006)
    - *SED not taken into account…*

Stecker & Salamon, ApJ 464, 600 (1996)

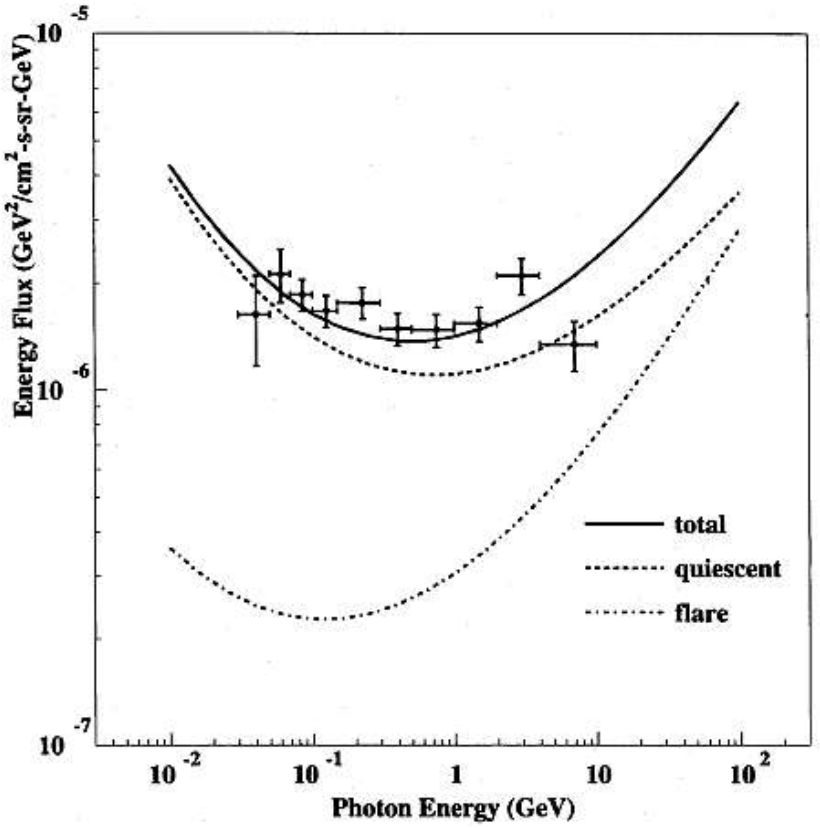

Blazar origin model of EGRB

Pavlidou & Venters, ApJ 673, 114 (2008)

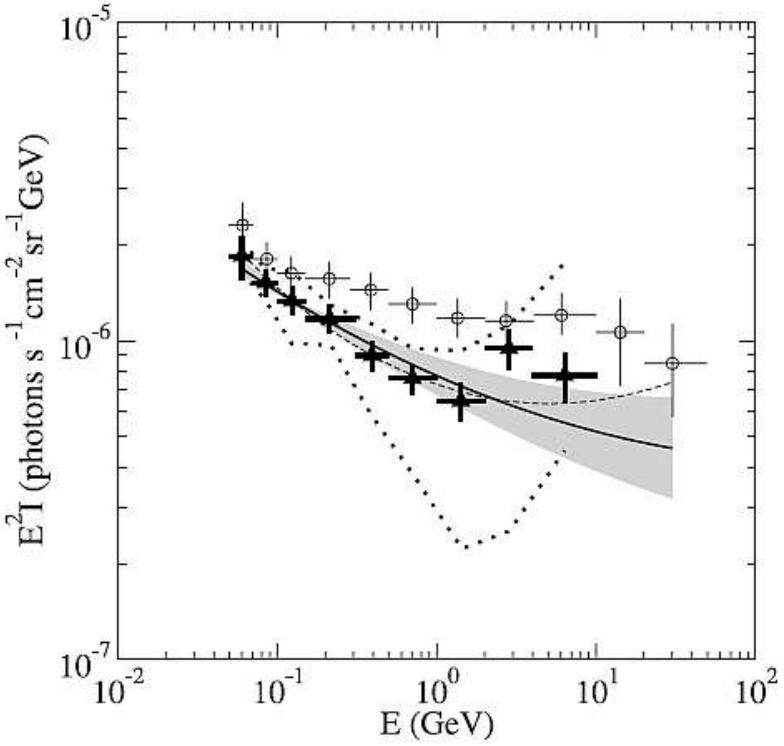

FIG. 1.—Spectral shape of the unresolved blazar emission. All curves have been normalized (arbitrarily) so that they pass through the 83 MeV point of the Strong et al. (2004) EGRB. *Solid line*: Best-guess spectrum based on a maximum-likelihood ISID determined using the Mattox et al. 2001 confident blazar sample. *Gray region*: Spectral shapes allowed for ISID parameters within the 1 σ likelihood contour. *Filled triangles*: Strong et al. (2004) EGRB determination. *Open circles*: Sreekumar et al. (1998) EGRB determination. Error bars are statistical errors only. *Thick dotted lines*: Strong et al. (2004) EGRB systematics. *Thin dotted line*: SID determined in Stecker & Salamon (1996a).

Kneiske & Mannheim, A&A 479, 41 (2008)

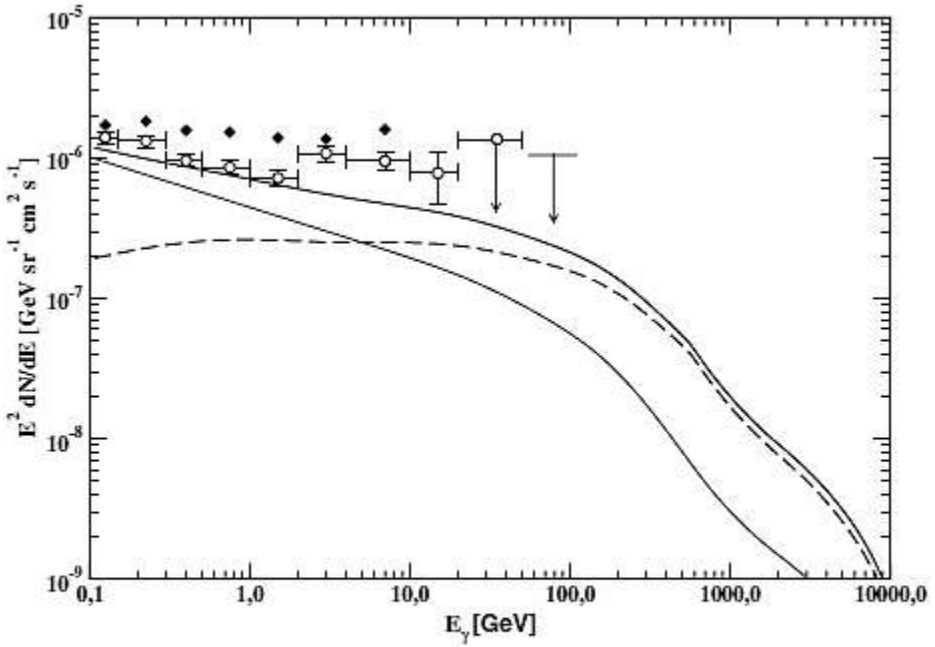

Fig. 6. Extragalactic gamma-ray background and assumed blazar contributions due to low-peaked blazars (thin solid line) and high-peaked blazars (dashed line) including the effects of intergalactic cascading.

Blazar SED sequence

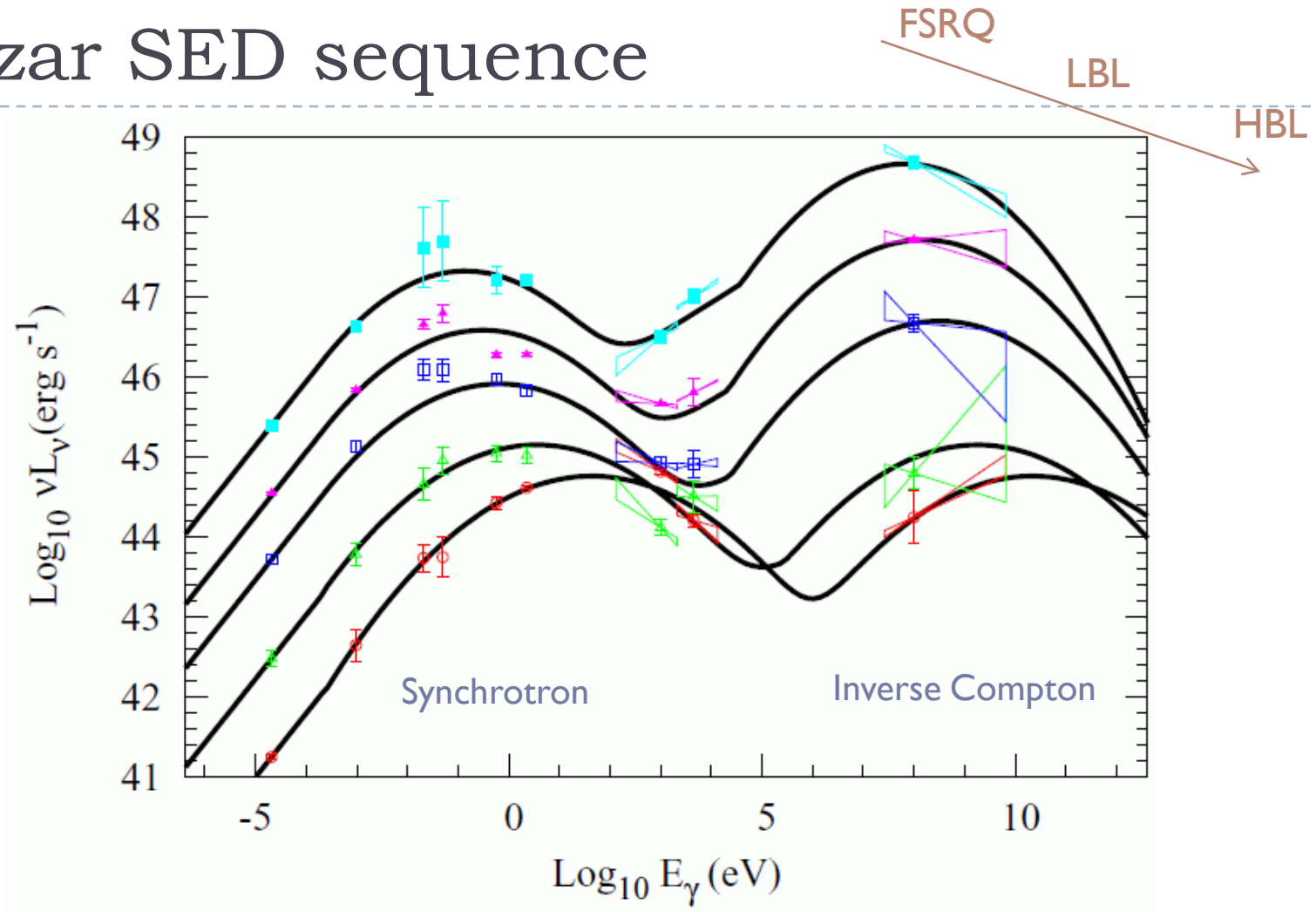

FIG. 1.— The blazar SED sequence. The data points are the average SED of the blazars studied by Fossati et al. (1998) and D01. The solid curves are the empirical SED sequence models constructed and used in this paper. The model curves corresponds to the bolometric luminosities of $\log_{10}(P/\mathrm{erg\ s^{-1}}) = 49.50$, 48.64, 47.67, 46.37, and 45.99 (from top to bottom).

Gamma-ray luminosity function model

- X-ray luminosity function (XLF) of AGN
  - LDDE (Luminosity-dependent density evolution) model
    - Peak redshift of density evolution increases with AGN luminosity
  - Assume (Bolometric luminosity of jet) $\propto$ (X-ray luminosity): $P = 10^{q} L_x$
  - X-ray bright AGNs used to derive XLF are close to Eddington limit (low Eddington ratio AGNs contribute less to GLF).
- Blazar gamma-ray luminosity function (GLF)

$$\rho_\gamma(L_\gamma,z) = \kappa(dL_X/dL_\gamma)\ \rho_X(L_X,z)$$ [κ: normalization factor]

$$\rho_X(L_X,z) = \rho_X(L_X,0)\ f(L_X,z)$$

$$\rho_X(L_X,0) = (A_X/L_X \ln(10))[(L_X/L_X^*)^{\gamma_1}+(L_X/L_X^*)^{\gamma_2}]^{-1}$$

$$f(L_X,z) = \begin{cases} (1+z)^{p_1} & : z<z_c(L_X) \\ f(L_X,z_c(L_X))[(1+z)/(1+z_c(L_X))]^{p_2} & : z>z_c(L_X) \end{cases}$$

$$z_c(L_X) = \begin{cases} z_c^* & : L_X > L_a \\ z_c^*(L_X/L_a)^{\alpha} & : L_X < L_a \end{cases} \qquad \begin{cases} p_1 = p_1^* + \beta_1(\log_{10}L_X - 44.0) \\ p_2 = p_2^* + \beta_2(\log_{10}L_X - 44.0) \end{cases}$$

GLF determined by EGRET blazars

- Gamma-ray flux

$$F_\gamma = \frac{1+z}{4\pi d_L(z)^2} \int_{\epsilon_{\min,\mathrm{obs}}(1+z)/h_p}^{\infty} \frac{L_\nu(\nu,P)}{h_p \nu} d\nu$$

- GLF model prediction

$$\frac{d^3N(z_i,F_{\gamma,i},\Omega_i)}{dz dF_\gamma d\Omega} = \frac{dV}{dz}\, \rho_\gamma(L_\gamma,z)\, \epsilon(F_\gamma,z) \times \Theta\lfloor F_\gamma - F_{\gamma,\mathrm{lim}}(\Omega)\rfloor,$$

- Likelihood function

$$\mathcal{L} = \prod_{i=1}^{N_{\mathrm{obs}}} \left\lfloor \frac{1}{N_{\mathrm{exp}}} \frac{dN(z_i,F_{\gamma,i},\Omega_i)}{dz dF_\gamma d\Omega} \right\rfloor$$

where

$$N_{\mathrm{exp}} = \int dz \int dF_\gamma \int d\Omega \frac{d^3N}{dz dF_\gamma d\Omega}$$

and $N_{\mathrm{exp}}=N_{\mathrm{obs}}=46$ ($\rightarrow\kappa$)

- Models
  - Ueda et al. (2003), Hasinger et al.(2005)
  - U03(q)
  - H05(q)
  - U03(q,γ_1)
  - H03(q,γ_1)

THE PARAMETERS OF THE AGN XLF

	Ueda et al. 2003	Hasinger et al. 2005
$A_X{}^a$	5.04×10^{-6}	2.62×10^{-7}
$\log_{10} L_X^{*\,b}$	$43.94^{+0.21}_{-0.26}$	43.94 ± 0.11
γ_1	0.86 ± 0.15	0.87 ± 0.10
γ_2	2.23 ± 0.13	2.57 ± 0.16
z_c^*	1.9^c	1.96 ± 0.15
$\log_{10} L_a{}^b$	44.6^c	44.67^c
α	0.335 ± 0.07	0.21 ± 0.04
p_1^*	4.23 ± 0.39	4.7 ± 0.3
p_2^*	-1.5^c	-1.5 ± 0.7
β_1	0.0^d	0.7 ± 0.3
β_2	0.0^d	0.6 ± 0.8

[a] In units of Mpc^{-3}.
[b] In units of ergs s^{-1}.
[c] These quantities are treated as fixed parameters in each XLF model.
[d] The indices β_1, β_2 are treated as constants in U03.

Comparison with EGRET blazars

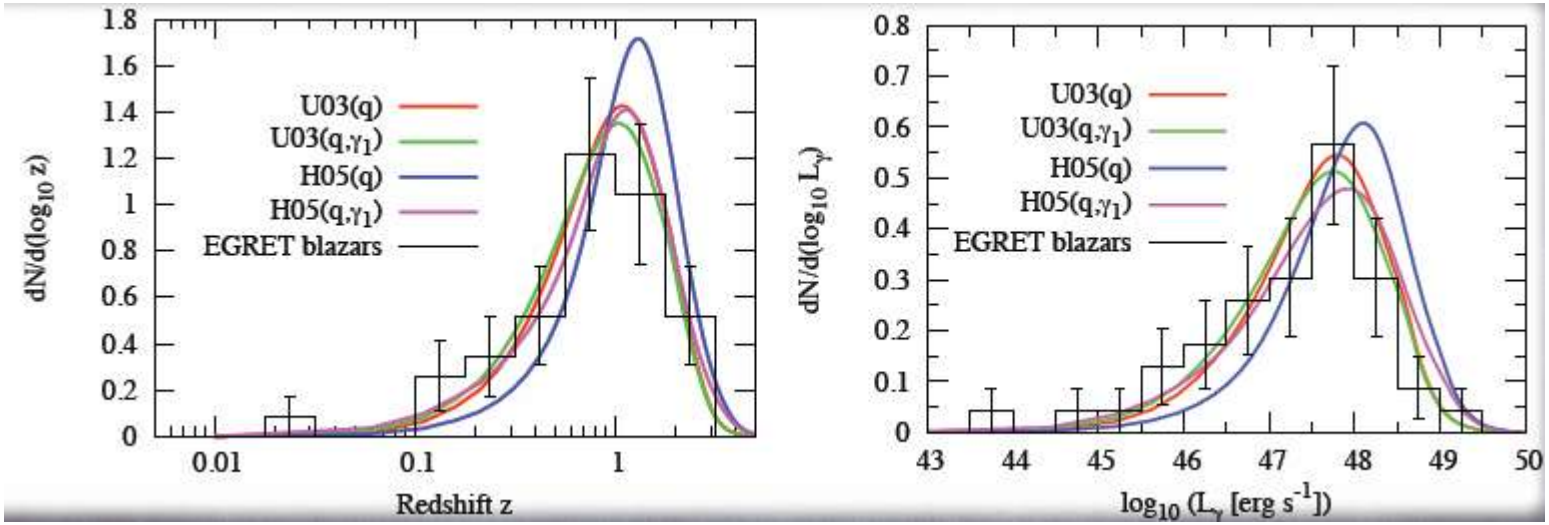

BEST-FIT PARAMETERS FOR BLAZAR GLF

	U03(q)	U03(q,γ_1)	H05(q)	H05(q,γ_1)
q	$4.92^{+0.21}_{-0.10}$	$4.93^{+0.25}_{-0.10}$	$5.29^{+0.26}_{-0.22}$	$5.35^{+0.25}_{-0.21}$
γ_1	0.86^{a}	0.93 ± 0.13	0.87^{a}	$1.11^{+0.11}_{-0.12}$
κ	1.7×10^{-6}	1.5×10^{-6}	9.5×10^{-6}	6.0×10^{-6}
		KS test probabilities		
z	53.8%	86.9%	0.15%	33.0%
L_γ	25.6%	48.4%	0.08%	28.5%

NOTE. — The best-fit values of the model parameters (q, γ_1, κ) obtained from the maximum likelihood analysis. The KS probabilities of the best-fit models are also shown for the redshift and gamma-ray luminosity distributions in the last two rows.

[a] These parameters are fixed at the original AGN XLF values in these analysis, and the fixed values are shown.

Allowed regions for U03/H05(q,γ_1) model

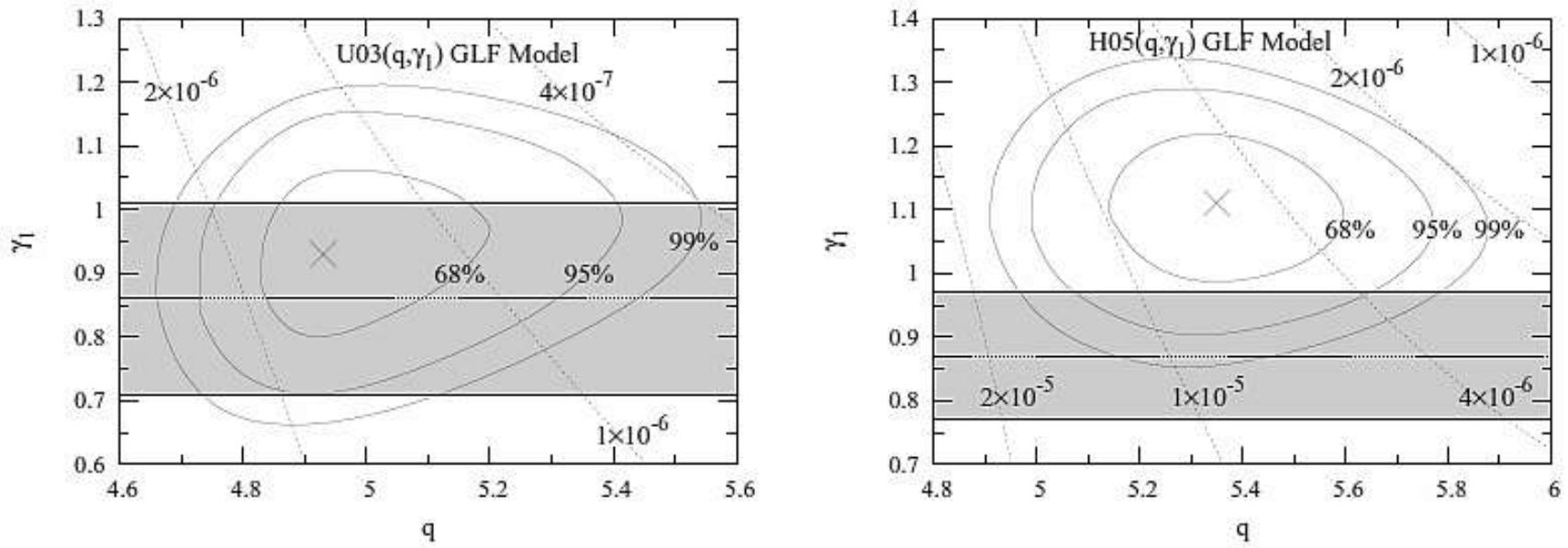

FIG. 3.— *Left*: Solid contours show the 68%, 95%, and 99% CL likelihood contours for the LDDE model parameters [the faint-end slope index, γ_1, and the ratio of the blazar emission power to X-ray luminosity, q] in the case of the U03 XLF. The best-fit values (q,γ_1)=(4.93, 0.93) are shown by the cross. The dotted contours are for the parameter κ, the normalization ratio of blazar GLF to AGN XLF. The κ values for the contours are indicated in the figure. The shaded region indicates the error region of the original γ_1 value determined for AGN XLF by X-ray surveys. *Right*: The same as the left panel, but for the H05 XLF. The best-fit values (q,γ_1)=(5.35, 1.11) are shown by the cross.

$L_{\rm jet,bol} \approx 10^5\, L_{\rm disk,X}$

AGN selection:
U03: hard X
H05: soft X

Good fit means that EGRET blazars are high-accretion rate AGNs.

Diffuse background spectrum (1)

- Integration of blazar SED sequence model in *z* and *L* space

$$\frac{d^2F(\epsilon_\gamma)}{d\epsilon_\gamma d\Omega} = \frac{c}{4\pi}\int_0^{z_{max}} dz \frac{dt}{dz}\int_{L_{min}}^{L_{max}} dL_\gamma\ \rho_\gamma(L_\gamma, z) \times \frac{(1+z)}{h_p}\frac{L_\nu[\epsilon_\gamma(1+z)/h_p, P(L_\gamma)]}{\epsilon_\gamma(1+z)} \times e^{-\tau_{\gamma\gamma}}(z, \epsilon_\gamma)\ ,$$

- $\tau(z,\varepsilon_\gamma)$: Totani & Takeuchi (2002)
  - Cascading effect:
    Pairs produced in $\gamma\gamma \rightarrow e^+e^-$ process scatter CMB photons
    Ref. Kneiske & Mannheim (2008)

Totani & Takeuchi ApJ 570, 470 (2002)

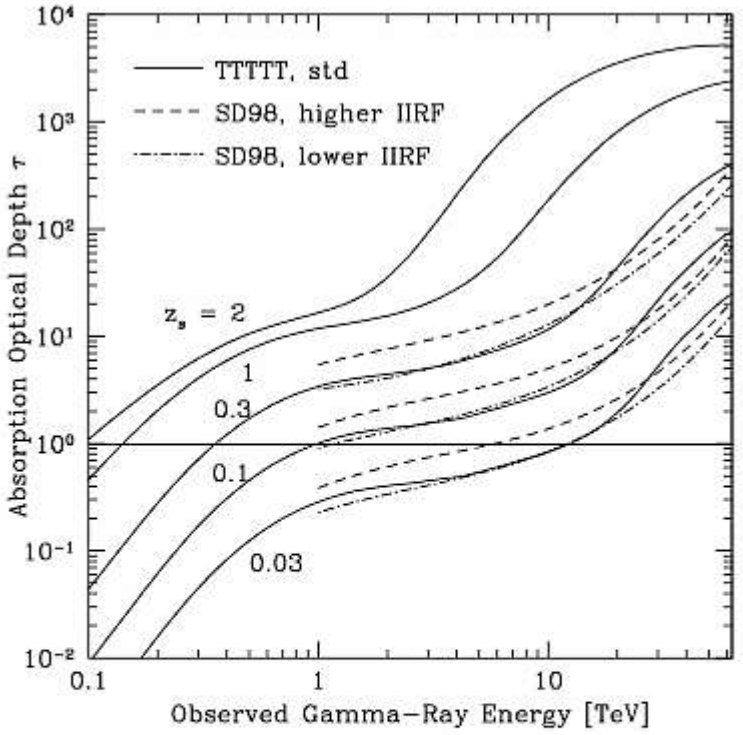

FIG. 19.—Intergalactic optical depth of very high energy gamma-rays to the absorption by interaction with optical/infrared cosmic background radiation as a function of the source redshift (z_s) and the gamma-ray energy observed at $z = 0$. The solid lines are the calculation based on our baseline model (indicated as TTTTT from the initials of the authors). The source redshifts are indicated in the figure. For comparison, calculations with "higher IIRF SED" (*dashed line*) and "lower IIRF SED" (*dot-dashed line*) by Stecker & de Jager (1998) are plotted for $z_s = 0.03$, 0.1, and 0.3 (*bottom to top*).

Diffuse background spectrum (2)

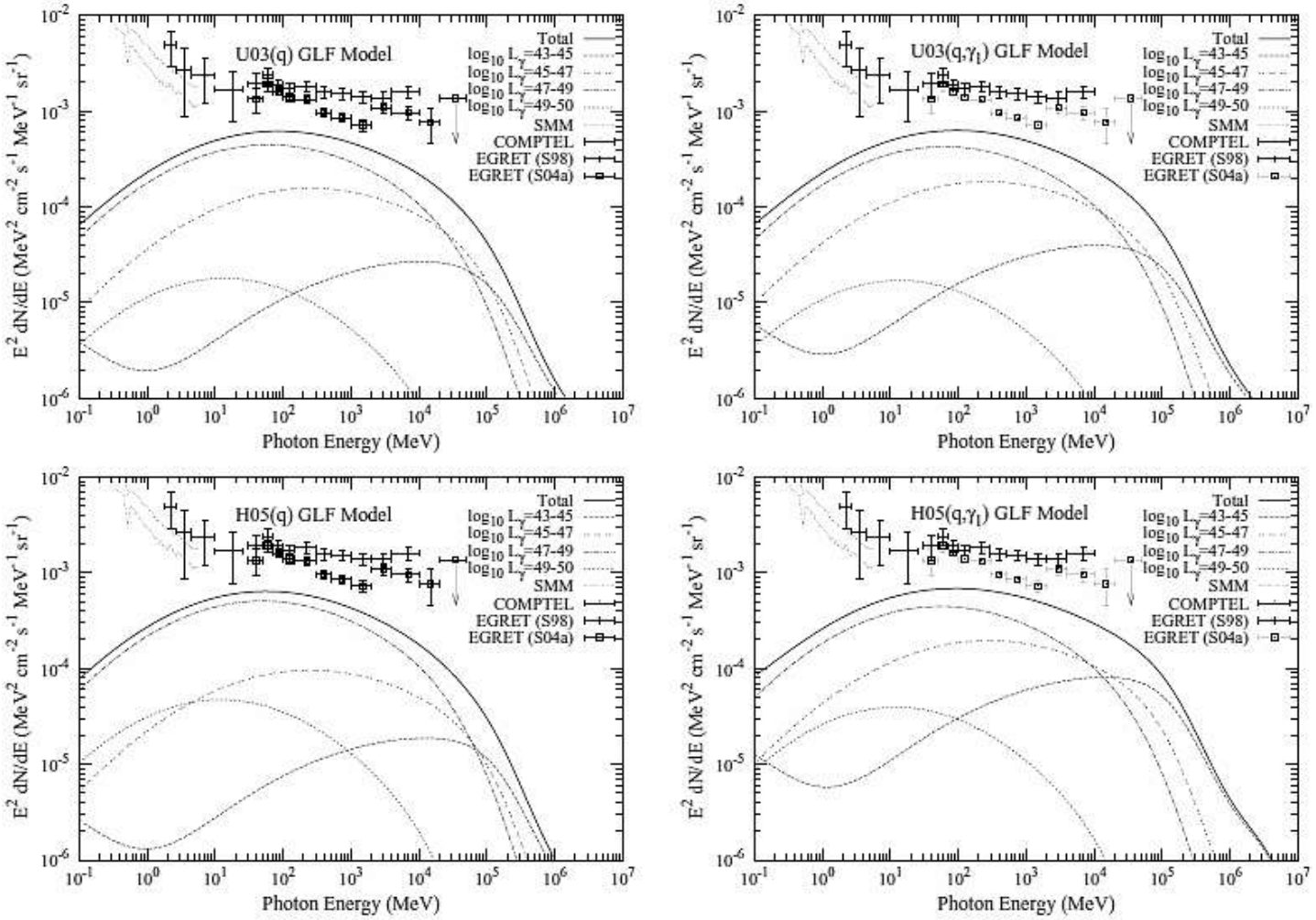

FIG. 4.— The blazar EGRB spectrum (energy flux per unit logarithmic photon energy and per steradian). The four panels are for the four different GLF models of U03(q), U03(q,γ_1), H05(q), and H05(q,γ_1). The solid curve is for the total EGRB spectrum from all blazars, and the other curves are for a particular range of blazar luminosity, as indicated in the figure (L_γ in units of erg/s). The effect of absorption by CIB is included, while the reprocessed cascade component is not included. The observed data of SMM (Watanabe et al. 1999), COMPTEL (Kappadath et al. 1996), and EGRET [Sreekumar et al. 1998 (S98); Strong et al. 2004a (S04a)] experiments are also shown with the symbols indicated in the figure.

Without cascading

Diffuse background spectrum (3)

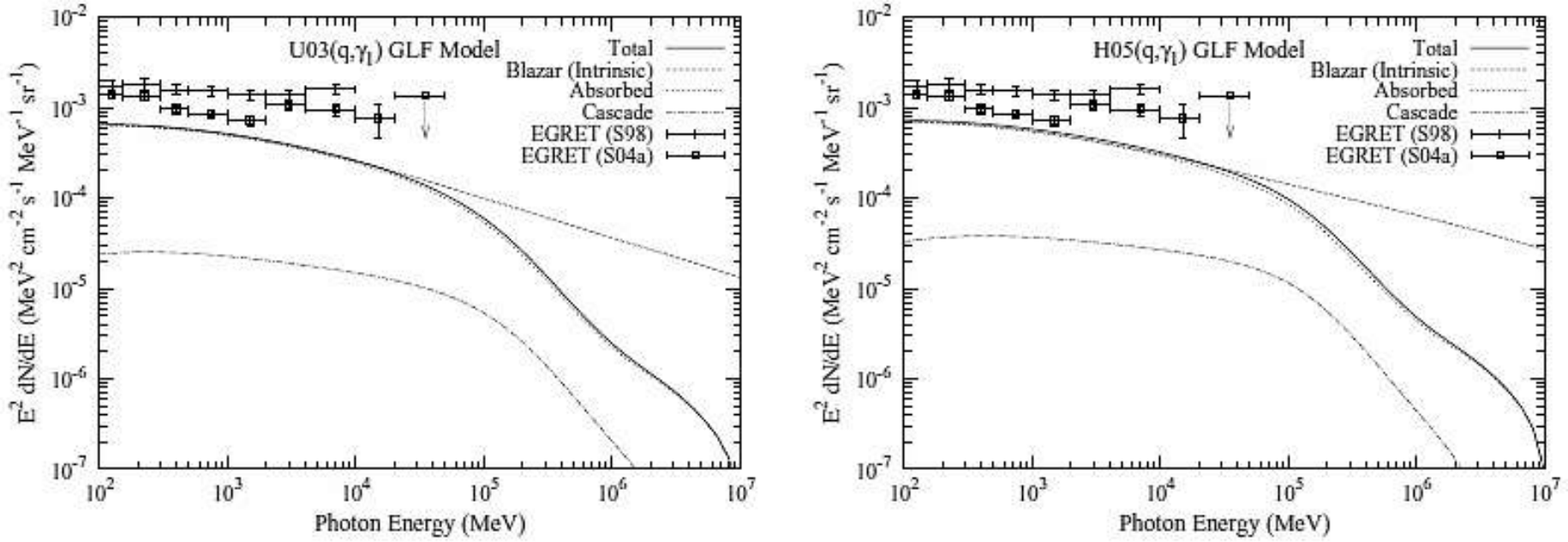

FIG. 5.— The blazar EGRB spectrum. The two panels are for the two different GLF models of U03(q,γ_1) and H05(q,γ_1). The curves are the model predictions for the intrinsic (no absorption by CIB), absorbed, and cascade (reprocessed emission by electrons/positrons produced in IGM) components of the EGRB spectrum. The solid curve is the total flux, i.e., absorbed plus cascade components. The EGRET data are the same as those in Fig. 4.

With cascading … does not alter the spectrum significantly

Diffuse background spectrum (4)

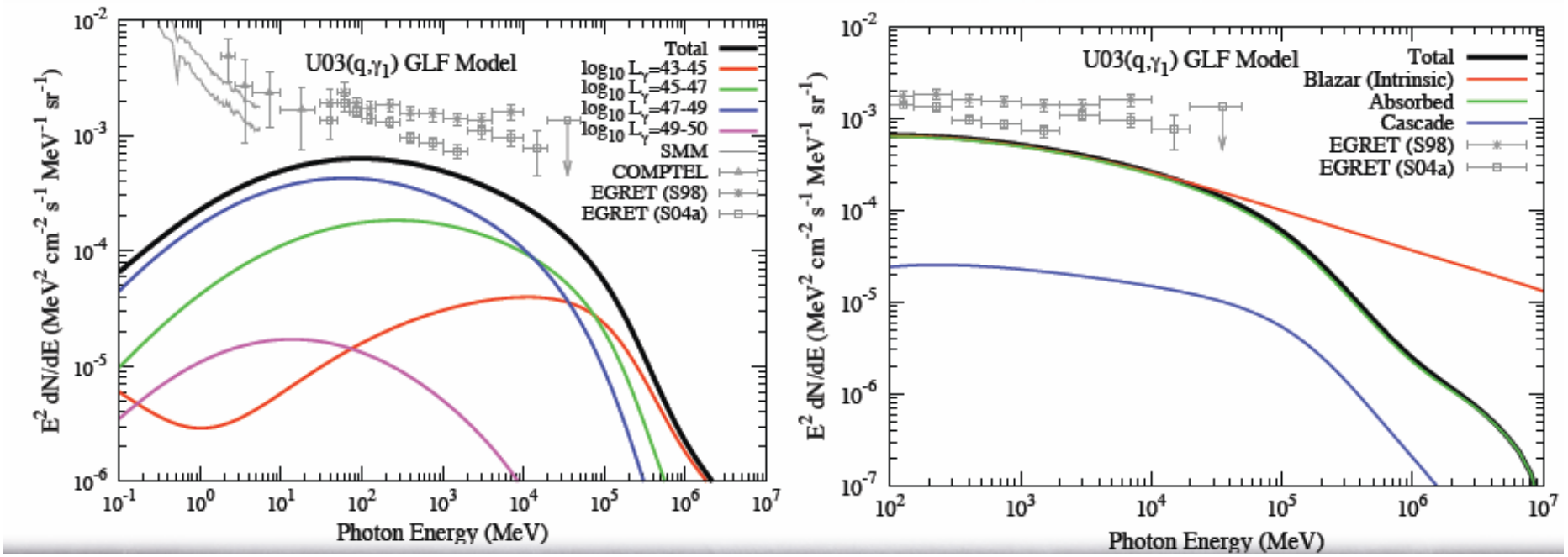

Note: MeV blazars are negligible in MeV background because of low population.

Diffuse background from non-blazars (1)

Non-thermal electrons in hot coronae around AGN accretion disks
→Non-thermal power-law component: X-ray to 1-10 MeV
[Inoue, Totani & Ueda, ApJ 672, L5 (2008)]

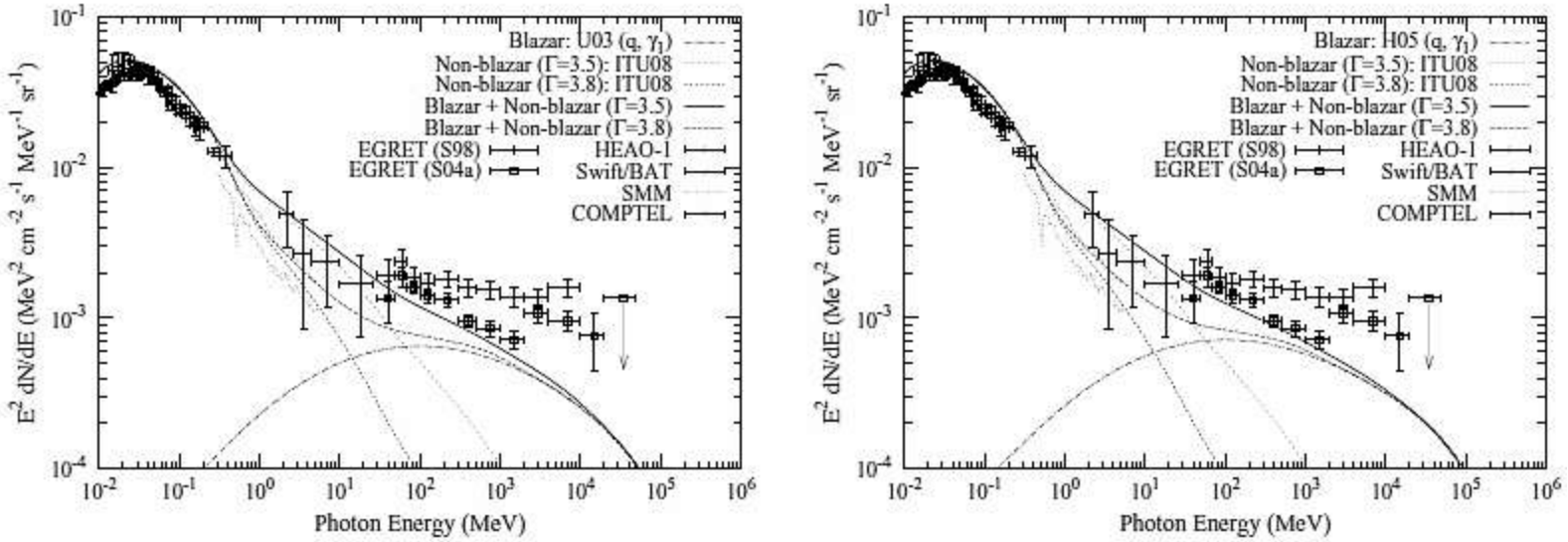

FIG. 6.— The EGRB spectrum from non-blazar AGNs and blazars. The two panels are for the two different blazar GLF models of U03(q, γ_1) (left) and H05(q, γ_1) (right). The model curves of the blazar component (absorbed+cascade), non-blazar AGN component, and the total of the two populations are shown. Note that two models are plotted for the non-blazar component with different values of Γ (see the line-markings indicated in the figure). The observed data of HEAO-1 (Gruber et al. 1999) and *Swift*/BAT (Ajello et al. 2008) are shown. The other data are the same as those in Fig. 4.

>100MeV: blazars are dominant sources
<100MeV: non-blazars

Diffuse background from non-blazars (2)

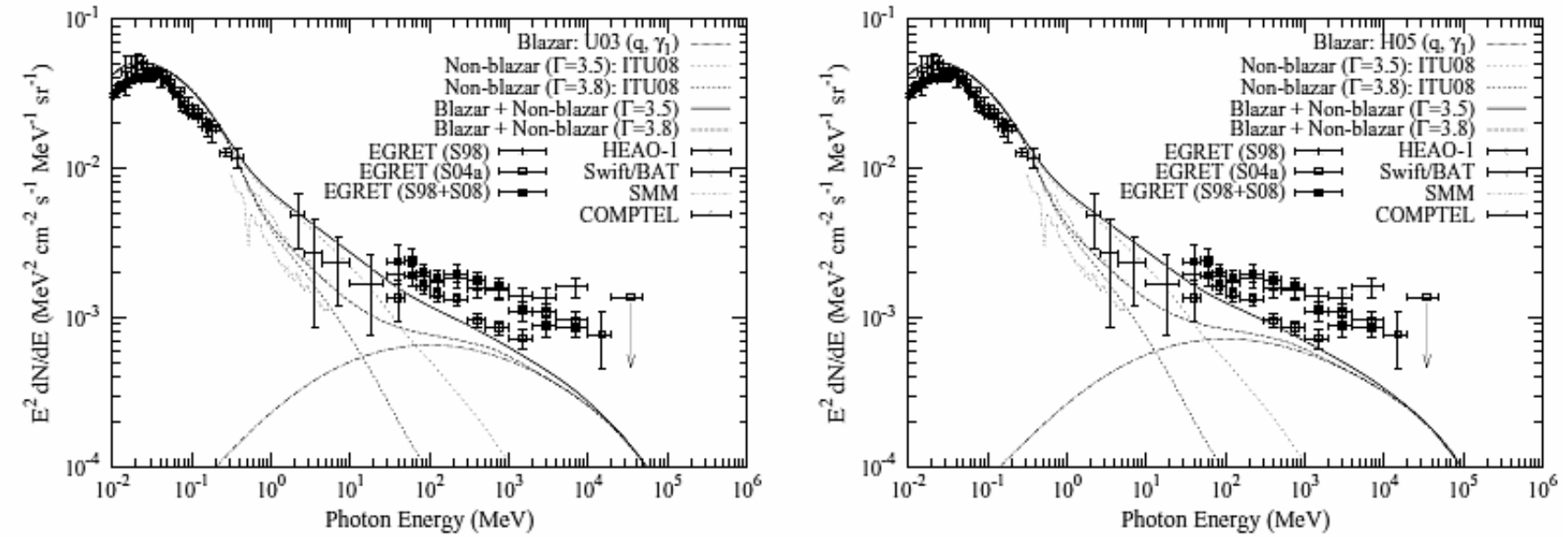

FIG. 7.— The same as Fig. 6, but with a new EGRET data denoted as "S98+S08", which is the original EGRET determination of Sreekumar et al. (1998) corrected by the correction factors proposed by Stecker et al. (2008, S08). The other data are the same as those in Fig. 4

>100 MeV: 30% from blazars
50% from non-blazars
20% ?? – systematics?

Flux distribution of blazars

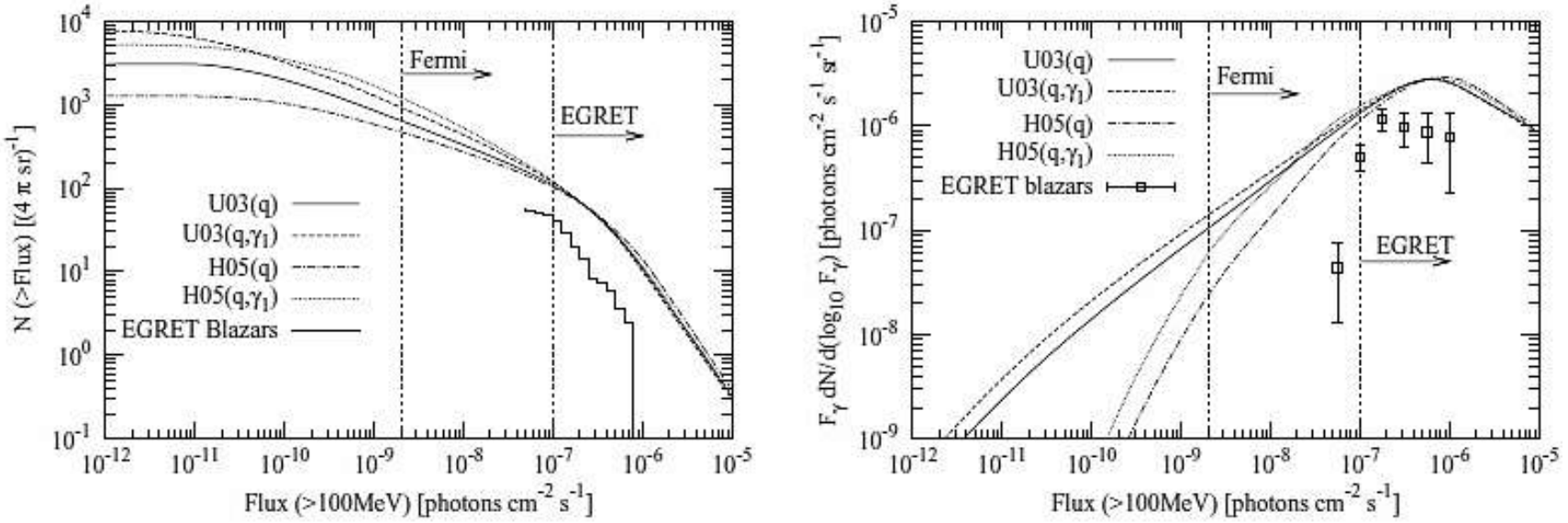

FIG. 8.— Left: the cumulative flux distribution of blazars. The four model curves correspond to the four different GLF models of U03(q), H05(q), U(q,γ_1), and H05(q,γ_1) are shown. The thin solid line shows the observed distribution of EGRET blazars. The detection limits of EGRET and *Fermi* are also shown. *Right*: the same as the left panel, but showing differential flux distribution multiplied by flux F_γ, to show the contribution to EGRB per logarithmic flux interval. The solid squares are the EGRET data with Poisson errors.

Fermi: 640 (U03(q))
930 (U03(q,γ_1))
470 (H05(q))
1,200 (H05(q,γ_1))

Cf. Stecker & Salamon 10,000
Narumoto & Totani 5,400 (PLE)
3,000 (LDDE)

Most of EGRB from blazars should be resolved by Fermi!

Flux distribution of blazars+non-blazars

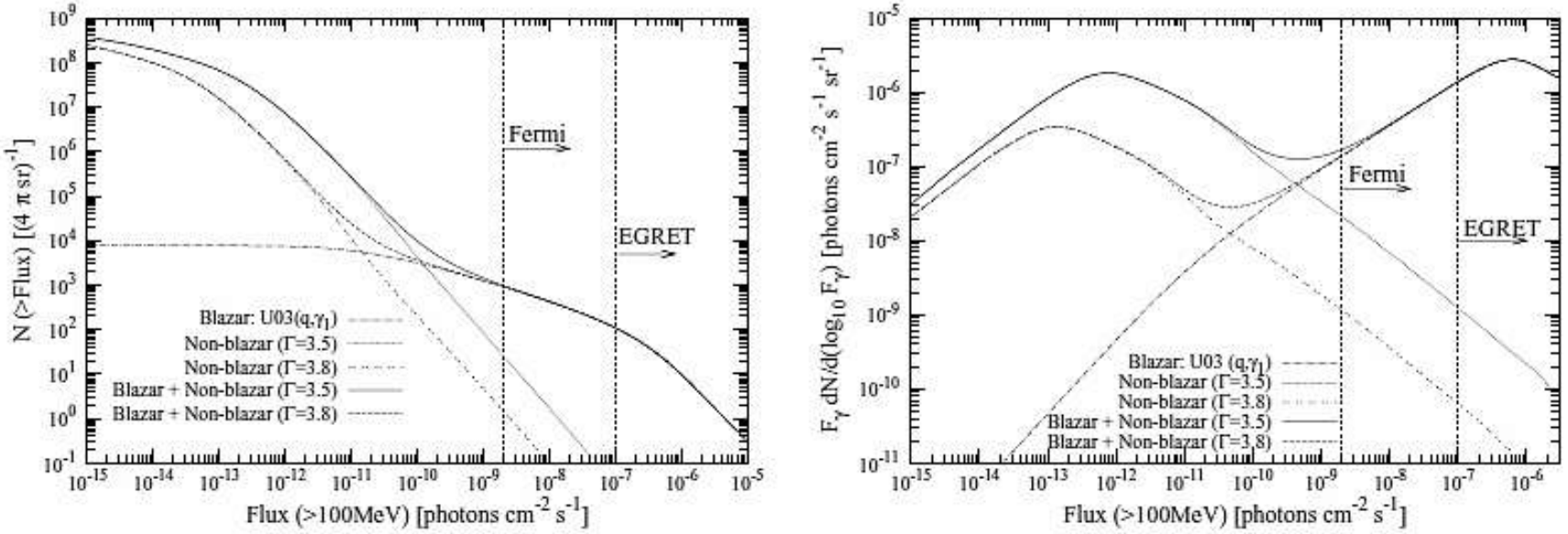

FIG. 9.— The same as Fig. 8, but showing non-blazar AGNs as well, in addition to blazars. The two models of non-blazar AGNs with different values of Γ are shown. The total of blazar plus non-blazar counts is also shown.

1-30 non-blazars would be detected by Fermi.
Ex. NGC4151… $(3\text{-}4)\times10^{-8}$cm^{-2}s^{-1}…
marginally detectable

Most of EGRB from non-blazars would be unresolved by Fermi.

At 100 MeV: $10^{48.0}$erg/s (blazars) & $10^{42.5}$erg/s (non-blazars)

Prediction: at ~100MeV considerable part of EGREB flux is unresolved

Fermi predictions

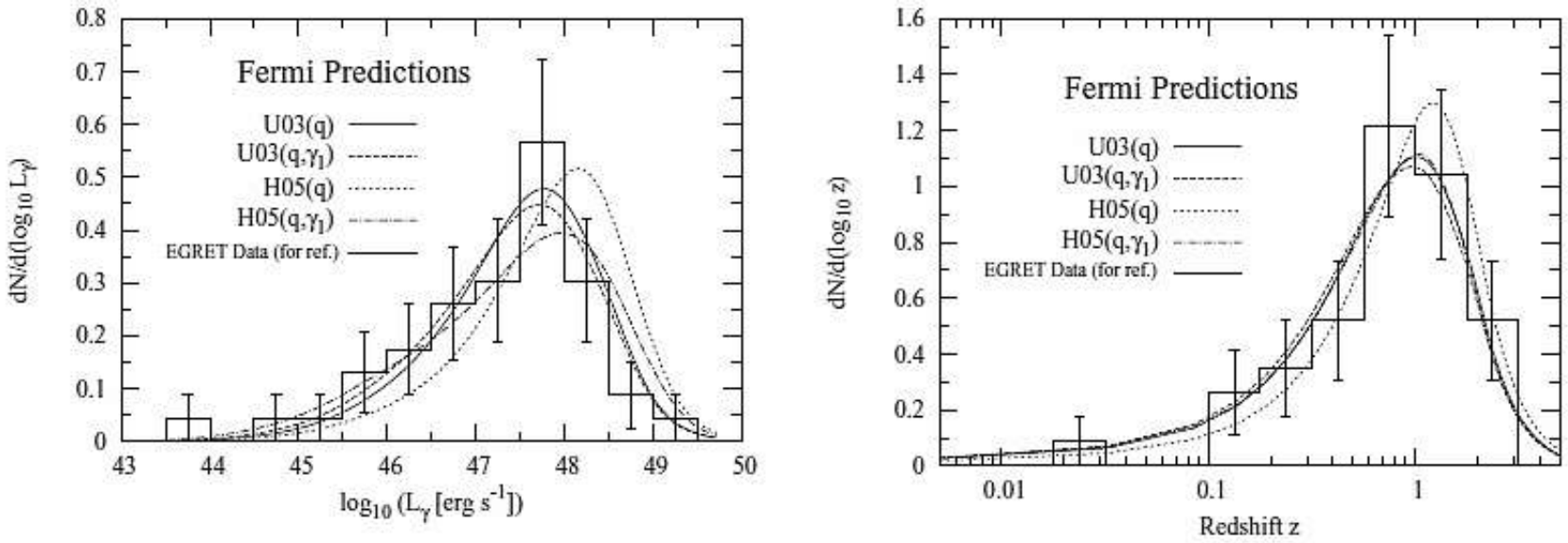

FIG. 10.— The predictions for the redshift and gamma-ray luminosity (νL_ν at rest frame 100 MeV) distributions of blazars for *Fermi*. The four model curves are for the four different GLF models of U03(q), H05(q), U(q,γ_1), and H05(q,γ_1). The *Fermi* sensitivity limit is set as $F_{\rm lim} = 2 \times 10^{-9}$ photons cm^{-2} s^{-1} for photon flux above 100 MeV. The observed distributions of EGRET blazars are shown, for comparison against the expected distributions of *Fermi* blazars.

Very similar to the case of EGRET…

Different GLF models can be tested by large statistics.

Conclusion

- Extragalactic background radiation spectrum was calculated by taking account of Blazar SED sequence.
- Spectrum below 10 GeV are not much affected by absorption with cosmic infrared background.
- Non-blazar contribution is significant in MeV region and considerable at 100 MeV.
- Blazars + non-blazars account for 80% of EGRB at 100 MeV and may be dominant.
- Hard spectrum observed above 1 GeV is not explained.
- 600-1200 blazars will be detected by Fermi above 100 MeV, which is smaller than previous studies.
- Prediction: above 1GeV most of EGRB flux will be resolved into discrete sources, while around 100 MeV significant fraction will be unresolved.